Inorganica Chimica Acta, 143 (1988) 259–270

Spectroscopic Study and Crystal Field Analysis of Eu^{3+} in the $YAl_3(BO_3)_4$ Huntite Matrix

C. GÖRLLER-WALRAND, P. VANDEVELDE, I. HENDRICKX

University of Leuven, Laboratory of Inorganic Chemistry, Celestijnenlaan 200F, B-3030 Heverlee, Belgium

P. PORCHER

Laboratoire des Eléments de Transition dans les Solides, E.R. 210 du CNRS, 1 Place A. Briand, 92195 Meudon Principal Cédex, France

J. C. KRUPA

Laboratoire de Radiochimie, Institut de Physique Nucléaire, F-91406 Orsay Cédex, France

and G. S. D. KING

University of Leuven, Laboratory of Crystallography, Celestijnenlaan 200C, B-3030 Heverlee, Belgium

(Received July 3, 1987)

Abstract

This study reports on the absorption, fluorescence and magnetic circular dichroism (MCD) spectra of $YAl_3(BO_3)_4$ doped with Eu^{3+}.

A crystal field analysis in the D_3 site symmetry group provided information on the energy levels and corresponding wave functions. Special emphasis is put on the power of the MCD technique for assessing the intensity mechanisms responsible for transitions between energy levels.

Introduction

Energy transfer between rare earth ions has been investigated in various matrices. Yttrium aluminium borate, isomorphous with the mineral huntite $Mg_3Ca(CO_3)_4$, is one of these. $YAl_3(BO_3)_4$ doped with Eu^{3+} has been extensively studied from the point of view of its luminescence properties, especially in connection with quenching processes [1–3].

The present study reports on more fundamental aspects of the spectroscopic properties of this complex in order to provide information on the energy levels and corresponding wave functions as well as on the intensity mechanisms involved in the transitions between these levels. These wave functions reflect the site symmetry of the Eu^{3+} system, which in turn allows interpretation of the spectroscopic features. The MCD technique is particularly interesting since it gives an excellent correlation between the site symmetry and the spectroscopy which accompanies this symmetry [4, 5]. Also the different controversies [2, 6] about the possible additional site symmetries for the Eu^{3+} ion can be partially resolved by the use of both fluorescence and magnetic circular dichroism techniques.

Experimental

The $Y_{1-x}Eu_xAl_3(BO_3)_4$ crystals (x = 0.9 and 0.1) were kindly given by Professor Blasse of the Rijksuniversiteit Utrecht (The Netherlands).

Crystal Structure Determination

The crystal structures of $Y_{1-x}Eu_xAl_3(BO_3)_4$ with x = 0.1 and 0.5 have been determined. As the variation in europium content had no effect on the structure within this range, it was not considered necessary to determine the structure of the compound with x = 0.9.

Diffraction measurements were carried out on a Syntex $P2_1$ diffractometer using graphite- monochromatized Mo Kα radiation (λ = 0.71073 Å). The crystals were of irregular form with diameter about 0.05 mm. Cell parameters were obtained by a least-squares analysis of the 2θ values of 24 reflections with 2θ between 20° and 30°. Intensities were measured by the ω–2θ scan method for half a reciprocal sphere out to $\sin\theta/\lambda$ = 1.1. An empirical absorption correction [7] was applied. Systematic absences ($-h + k + l \neq 3n$) were compatible with the space group $R32$. The structures were solved by Patterson methods and refined by full-matrix least-squares methods. All calculations were carried out using the X-ray 76 system [8]. Details of the structure determination are given in Table I. Figure 1a is an ORTEP [9] drawing of the structure projected along the c axis. Figure 1b shows the lanthanide environment, a distorted trigonal prism of crystal-

0020-1693/88/$3.50

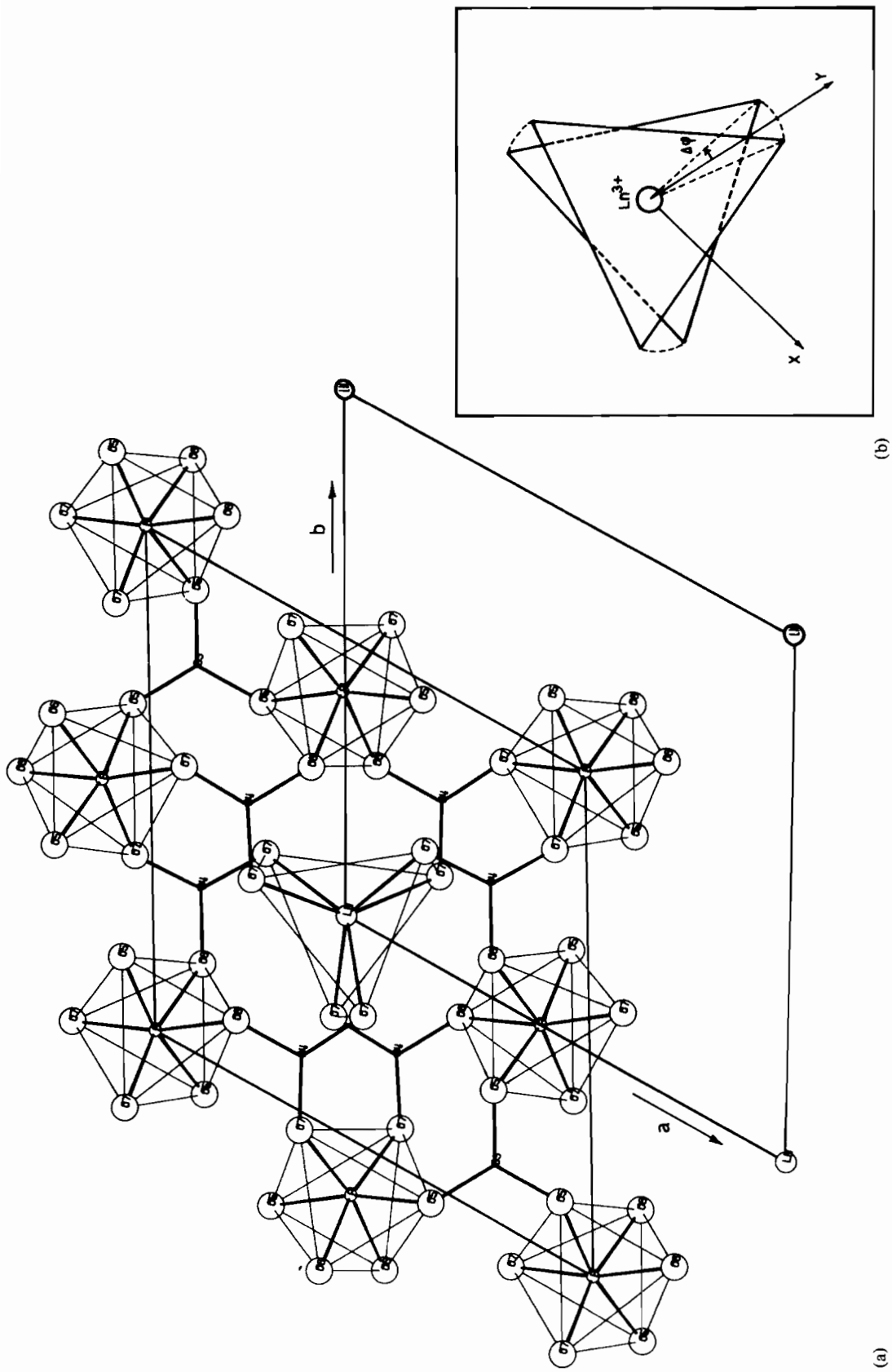

(a) (b)

Fig. 1. (a) Crystal structure of $LnAl_3(BO)_3)_4$ (projection perpendicular to *c*-axis). (b) Coordination polyhedron around the Ln^{3+} ion (projection perpendicular to *c*-axis).

TABLE I. Crystal Structure of $Y_{1-x}Eu_xAl_3(BO_3)_4$[a]

		$x = 0.1$	$x = 0.5$
a (Å)		9.2833(7)	9.2945(7)
c (Å)		7.2331(6)	7.2491(7)
μ (λ = 0.71073 Å) cm^{-1}		78.8	88.4
Reflections measured		8342	8344
Unique reflections ($I > 3\sigma(I)$)		748	749
Observed reflections		687	677
$R = \Sigma\|\|F_o\| - \|F_c\|\|/\Sigma\|F_o\|$			
all reflections		0.024	0.033
observed reflections		0.022	0.032
Atomic parameters			
Y	x	0	0
	y	0	0
	z	0	0
	U_{eq} (Å^2)[b]	0.0043(2)	0.0020(2)
Al	x	0	0
	y	0.4444(2)	0.4429(4)
	z	0	0
	U_{eq} (Å^2)	0.0049(3)	0.0052(7)
B(3)	x	1/3	1/3
	y	2/3	2/3
	z	1/6	1/6
	U_{eq} (Å^2)	0.0049(8)	0.0047(22)
B(4)	x	1/3	1/3
	y	0.2240(7)	0.2262(23)
	z	1/6	1/6
	U_{eq} (Å^2)	0.0047(9)	0.0038(34)
O(5)	x	1/3	1/3
	y	0.8156(4)	0.8158(10)
	z	1/6	1/6
	U_{eq} (Å^2)	0.0046(5)	0.0048(15)
O(6)	x	1/3	1/3
	y	0.0754(5)	0.0752(16)
	z	1/6	1/6
	U_{eq} (Å^2)	0.0064(7)	0.0090(27)
O(7)	x	0.1834(3)	0.1843(9)
	y	0.2170(3)	0.2179(9)
	z	0.1871(4)	0.1897(9)
	U_{eq} (Å^2)	0.0062(6)	0.0059(18)

[a]Figures in parentheses give standard deviations in units of the last figure. Space group $R32$, $Z = 3$. [b]$U_{eq} = \Sigma U_{ij} a_i^* a_j^* a_i \cdot a_j$ is the equivalent isotropic vibration parameter for the anisotropic parameters U_{ij}.

lographic symmetry D_3. The non-zero distortion angle ($\Delta\varphi = 8.3°$) prevents the prism from having the higher non-crystallographic symmetry D_{3h}.

Spectroscopic Measurements

Polarization spectra

The spectra were recorded at room temperature with a Cary 219 spectrophotometer and at liquid nitrogen temperature with a McPherson spectrophotometer (1200 lines/mm). Some spectra were recorded at liquid helium temperature in the Institut de Physique Nucléaire at Orsay with a HR 1000 Jobin Yvon monochromator (1200 lines/mm in the UV–Vis and 600 lines/mm in the IR).

Three spectra were recorded: parallel to the crystal c-axis (α-spectrum), perpendicular to the c-axis with the electric vector first parallel (π-spectrum) and then perpendicular (σ-spectrum) to the c-axis.

Fluorescence spectra

The fluorescence spectra were excited either by a Hg lamp or by a dye laser (Rhodamine 6 G) pumped by a 4W argon laser (Spectra Physics). The fluorescence light was analysed with a Jarrell–Ash monochromator. Measurements at 77 K were performed with an Oxford cryostat.

MCD spectra

The MCD equipment consisted essentially of a McPherson monochromator (1200 lines/mm) a Hinds modulator and a 7 Tesla supermagnet. The spectra were recorded at 77 K.

TABLE II. Full Rotation Compatibility Table of the Group D_3

J	Irreducible representation
0	A_1
1	$A_2 + E$
2	$A_1 + 2E$
3	$A_1 + 2A_2 + 2E$
4	$2A_1 + A_2 + 3E$
5	$A_1 + 2A_2 + 4E$
6	$3A_1 + 2A_2 + 4E$

Results and Discussion

Polarization Spectra

The polarization spectra have partly been published previously [10]. These data dealt with the $^5D_{0,1,2,3} \leftarrow {}^7F_{0,1,2}$ transitions. We discuss here the transitions to $^5L_6$ and $^7F_6$.

Use is made of Tables II and III giving the splitting of the $^{2S+1}L_J$ levels up to $J = 6$ in D_3 and the selection rules for electric and magnetic dipole transitions for D_3 symmetry.

$^5L_6 \leftarrow {}^7F_0$ *(Fig. 2a)*

Because of the large overlapping of the bands at room temperature, the sample was cooled to 4.2 K so that only the transitions from $^7F_0$ appear. The splitting of the $^5L_6$ level in D_3 is given in Table II.

From $^7F_0(A_1)$ two electric dipole transitions are expected to be polarized in π while four others are polarized in σ. That this is indeed the case is shown experimentally in Fig. 2a.

TABLE III. Selection Rules for Electric and Magnetic Dipole Transitions in D_3 Symmetry

ED	A_1	A_2	E	MD	A_1	A_2	E
A_1		π	$\sigma + \alpha$	A_1		σ	$\pi + \alpha$
A_2	π		$\sigma + \alpha$	A_2	σ		$\pi + \alpha$
E	$\sigma + \alpha$	$\sigma + \alpha$	$\sigma + \pi + \alpha$	E	$\pi + \alpha$	$\pi + \alpha$	$\sigma + \pi + \alpha$

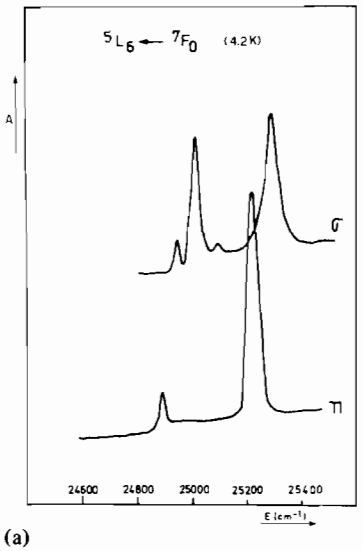

(a)

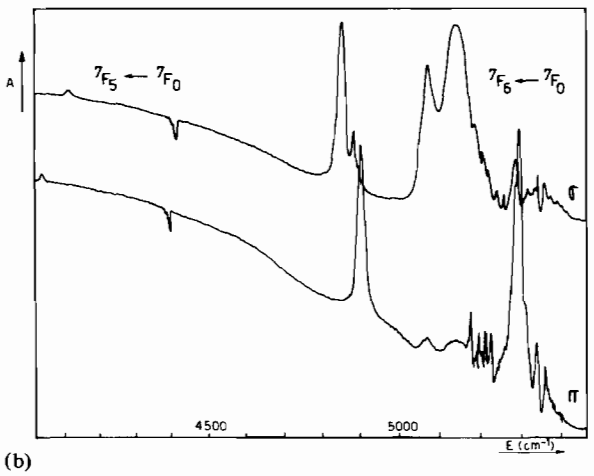

(b)

Fig. 2. Polarization spectra (see also ref. 10). (a): $^5L_6 \leftarrow {}^7F_0$ transition (4.2 K); (b) $^7F_6 \leftarrow {}^7F_0$ transition (4.2 K).

Because of the forbidden character of the $A_1 \leftarrow A_1$ transition, this spectrum gives us no information about the A_1 energy levels.

$^7F_6 \leftarrow {}^7F_0$ (Fig. 2b)

Theoretically, the same selection rules hold true for this transition as the $^5L_6 \leftarrow {}^7F_6$ one, as is shown in Fig. 2b.

Fluorescence Spectra

Our results largely support the work of Kellendonk and Blasse [2] and can be summarized as follows.

$^5D_0 \rightarrow {}^7F_1$

This magnetic dipole transition reproduces the same splitting pattern as the $^5D_1 \leftarrow {}^7F_0$ transition in absorption (two lines in view of the D_3 symmetry). One is found at 16 892 cm^{-1} and the other at 16 762 cm^{-1}.

$^5D_0 \rightarrow {}^7F_2$

The two lines expected to be predominant in the electric dipole mechanism are indeed found (16 284 and 16 166 cm^{-1}).

$^5D_0 \rightarrow {}^7F_3$

This transition is electric and magnetic dipole forbidden. However, through configuration interaction some allowed character is induced resulting in four lines that are indeed detected at 15 394, 15 336, 15 276 and 15 250 cm^{-1}.

$^5D_0 \rightarrow {}^7F_4$

The four lines predicted from the electric dipole mechanism appear predominantly at 14 679, 14 619, 14 308 and 14 206 cm^{-1}.

Remarks

(i) In all the cases mentioned above we observed the presence of the satellite peaks described by Kellendonk and Blasse [2]. However, on selective excitation of the $^5D_0$ level, only the lines due to the regular Eu^{3+} site remain.

(ii) The transition $^5D_0 \rightarrow {}^7F_0$ is electric and magnetic dipole forbidden within a D_3 symmetry. Nevertheless, two lines are observed (17 150 and 17 070 cm^{-1}). Only the selective excitation of the 17 150 cm^{-1} line results in an emission spectrum, which shows the same features as the spectrum due to the regular Eu^{3+} site. The satellite peaks which appear in the UV spectrum are not present in these spectra. In this way, the possibility, claimed by Kellendonk and Blasse of a C_2-site for the Eu^{3+} ions is not confirmed in these spectra. The $^5D_0 \rightarrow {}^7F_0$ line is due to a lowered D_3 symmetry transition.

The energy level scheme that takes the absorption and fluorescence data into account is shown in Fig. 3.

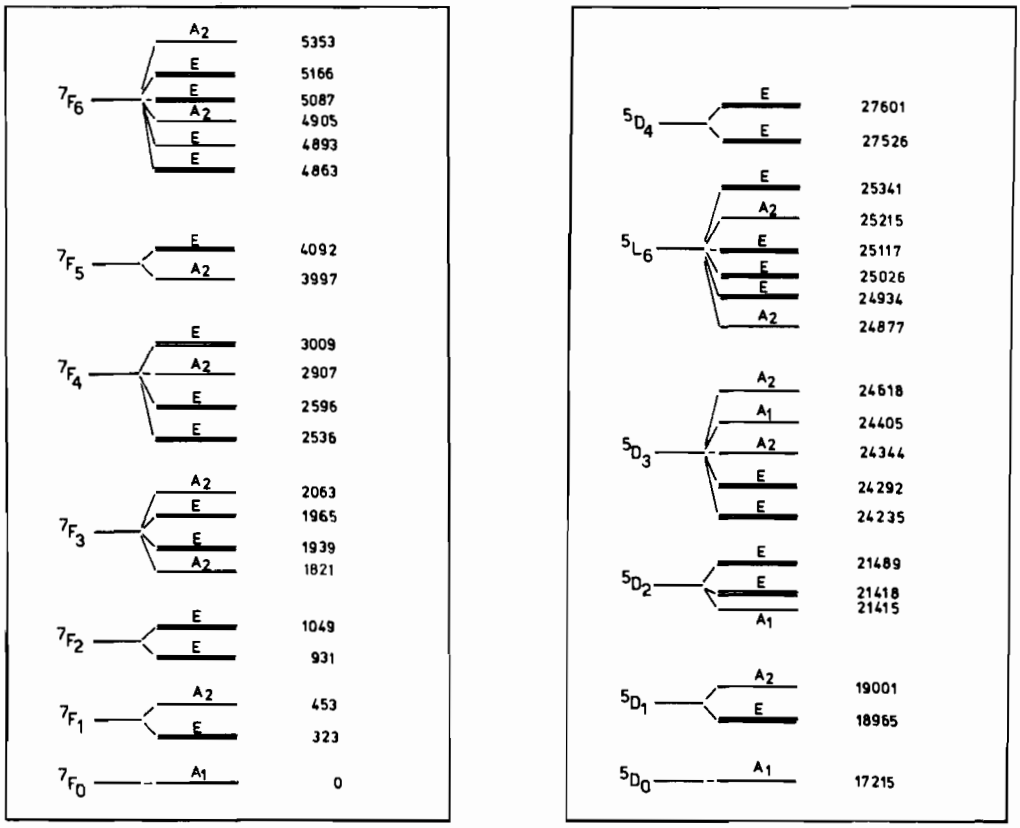

Fig. 3. Energy diagram of the doped $YAl_3(BO_3)_4/Eu^{3+}$.

The corresponding wave numbers and polarization mechanisms based on the comparison of absorption and fluorescence data are given in Table IV.

Crystal Field Parametrization

From the previous section, 36 levels have been identified. Despite the fact that this is relatively few compared to those considered in fitting spectra of ions like Er^{3+} and Ho^{3+} [11], we have nevertheless made a crystal field fitting with a view to substantiating the MCD results discussed in the next section. Use was made of the D_3 Hamiltonian:

$$\mathcal{H}'_{D_3}\,(\text{even}) = B_0^2 C_0^{(2)} + B_0^4 C_0^{(4)} + B_3^4 (C_{-3}^{(4)} - C_{+3}^{(4)}) + B_0^6 C_0^{(6)} + B_3^6 (C_{-3}^{(6)} - C_{+3}^{(6)}) + B_6^6 (C_{-6}^{(6)} + C_{+6}^{(6)})$$

For the calculation the following points were taken into account:

(i) As the ^7F multiplet is well isolated in the energy level scale (the $^5D_0$ to $^7F_6$ difference amounts to 12000 cm^{-1}), the ^7F wave functions may be supposed to be relatively pure (>90%). Moreover, the crystal field operator acts only on states with the same multiplicity: the ^7F_J multiplet is the only septet of the configuration, and therefore it is reasonable to use the reduced base of the $49|^7F_{JM}>$ states in the first calculations. In the second place, the basis set will be arbitrarily extended to 200 to simulate the ^5D_J levels.

(ii) The simulation of the energy level scheme involves six experimental crystal field parameters. The automatic refining procedure minimizes the r.m.s. deviation. A knowledge of the rough values of the parameters, which can be used as starting parameters, facilitates the refinement. Two refinements, from two sets of departure values, were performed:

(a) From lattice sum calculations

Crystal field parameters were determined by the method described by Leavitt and Morrison [12, 13] where B_q^k values are related to the lattice sum A_q^k values by

$$B_q^k = (1 - \sigma_k)\,\frac{\langle r^k \rangle}{\tau^k} A_q^k$$

where σ_k is a screening factor, $\langle r^k \rangle$ the value of the radial integral and τ^k an expansion coefficient for $\langle r^k \rangle$. The effective charges were the ionic charge for aluminium and yttrium, 1.5 for boron and 1.5 for oxygen. The last two take partial account of the covalent nature of the D_3 entity.

TABLE IV. Identification of the Electronic Transitions in the Absorption and Fluorescence Spectrum of $YAl(BO_3)_4/Eu^{3+}$

Absorption energy (cm^{-1})	Polarization	Mechanism	Identification	
3997	χ	ED	$^7F_5 \leftarrow {}^7F_0$	$A_2 \leftarrow A_1$
4092	σ	ED		$E \leftarrow A_1$
4863	σ	ED		$E \leftarrow A_1$
4893	σ	ED		$E \leftarrow A_1$
4905	π	ED	$^7F_6 \leftarrow {}^7F_0$	$A_2 \leftarrow A_1$
5087	σ	ED		$E \leftarrow A_1$
5166	σ	ED		$E \leftarrow A_1$
5353	π	ED		$A_2 \leftarrow A_1$
16166	σ	ED	$^5D_0 \leftarrow {}^7F_2$	$A_1 \leftarrow E$
16284	σ + α	ED		$A_1 \leftarrow E$
16762	σ	MD	$^5D_0 \leftarrow {}^7F_1$	$A_1 \leftarrow A_2$
16892	π + α	MD		$A_1 \leftarrow E$
17916	σ + π	ED of MD		
17952	σ	ED of MD	$^5D_1 \leftarrow {}^7F_2$	
18034	σ + π	ED of MD		$E \leftarrow E$
18070	σ + π	ED of MD		
18512	σ	ED	$^5D_1 \leftarrow {}^7F_1$	$E \leftarrow A_2$
18642	σ + α	ED		$E \leftarrow E$
18678	σ	ED		$A_2 \leftarrow E$
18965	π + α	MD	$^5D_1 \leftarrow {}^7F_0$	$E \leftarrow A_1$
19001	σ	MD		$A_2 \leftarrow A_1$
20962	σ + α	ED of MD	$A_1 \leftarrow A_2$	$E \leftarrow A_2$
21036	σ + π	ED	$^5D_2 \leftarrow {}^7F_1$	$E \leftarrow A_2$
21086	σ + π	ED of MD	$A_1 \leftarrow E$	$E \leftarrow E$
21164	σ + π	ED		$E \leftarrow E$
21418	σ + α	ED	$^5D_2 \leftarrow {}^7F_0$	$E \leftarrow A_1$
21489	σ + α	ED		$E \leftarrow A_1$
23839	σ	ED		$E \leftarrow A_2$
23912	π	ED		$E \leftarrow E$
23952	π	ED		$A_1 \leftarrow A_2$
23969	σ + π + α	ED	$^5D_3 \leftarrow {}^7F_1$	$E \leftarrow E$
24021	σ + α	ED		$A_2 \leftarrow E$
24082	σ	ED		$A_1 \leftarrow E$
24295	σ	ED		$A_2 \leftarrow E$
24877	π	ED		$A_2 \leftarrow A_1$
24934	σ + α	ED		$E \leftarrow A_1$
25026	σ + α	ED	$^5L_6 \leftarrow {}^7F_0$	$E \leftarrow A_1$
25117	σ	ED		$E \leftarrow A_1$
25215	π	ED		$A_2 \leftarrow A_1$
25341	σ + α	ED		$E \leftarrow A_1$
27073	σ + π	ED of MD		$E \leftarrow A_2$
27148	σ	ED		$E \leftarrow A_2$
27196	σ + π	ED of MD	$^5D_4 \leftarrow {}^7F_{0,1}$	$E \leftarrow E$
27278	σ + π	ED of MD		$E \leftarrow E$
27526	σ + π	ED of MD		$E \leftarrow A_1$
27601	σ + π	ED of MD		$E \leftarrow A_1$

Fluorescence energy (cm^{-1})	Idendification	Remarks
17150	$^5D_0 \rightarrow {}^7F_0$ $A_1 \rightarrow A_1$	
17070		
16927		b
16913		b

(continued)

TABLE IV. *(continued)*

Fluorescence energy (cm^{-1})	Identification		Remarks
16892		$A_1 \rightarrow E$	
16886	$^5D_0 \rightarrow {}^7F_1$		
16874			b
16778			b
16762		$A_1 \rightarrow A_2$	
16346			b, c
16284		$A_1 \rightarrow E$	
16258	$^5D_0 \rightarrow {}^7F_2$		b, c
16166		$A_1 \rightarrow E$	
16100			b,c
15394		$A_1 \rightarrow A_2$	
15336	$^5D_0 \rightarrow {}^7F_3$	$A_1 \rightarrow A_2$	c
15276		$A_1 \rightarrow E$	
15250		$A_1 \rightarrow E$	
14692			
14679		$A_1 \rightarrow E$	
14630			
14626			b, c
14619	$^5D_0 \rightarrow {}^7F_4$	$A_1 \rightarrow E$	
14525			b, c
14467			b, c
14308		$A_1 \rightarrow A_2$	
14206		$A_1 \rightarrow E$	b

[b]Disappears by selective excitation (λ = 5830.9 Å) ($^5D_0 \leftarrow {}^7F_0$). [c]Disappears by selective excitation (λ = 5917.5 Å) ($^5D_0 \leftarrow {}^7F_1$).

(b) From the descending symmetry procedure [14]

The procedure considers the crystallographic evidence that the real site symmetry D_3 is not far from D_{3h}, where the number of parameters is only four: B_0^2, B_0^4, B_0^6 and B_6^6. Moreover, for the particular case of the $4f^6$ configuration, the splitting of $^7F_1$ in the first order only depends on B_0^2, and the splitting of $^7F_2$ depends to a first approximation only on B_0^2 and B_0^4. This allows us to estimate rough values of B_0^2 and B_0^4. Thus other parameters are estimated by looking at the splitting of other ^7F_J levels (mainly $^7F_6$ in our case). When the refinement is achieved for D_{3h}, extra parameters, namely B_3^4 and B_3^6 are added, corresponding to the lowering in symmetry.

Two sets of final parameters were determined with a good accuracy (see Table V). It is rather curious that the extra parameters B_3^4 and B_3^6 are not negligible in spite of the real symmetry being very near to D_{3h}. For the first type of refinement B_3^6 is also very far from the starting value. An evaluation of the two sets is given in Table V.

In Table VI, the calculated energy levels are given with the experimental ones for the ^7F multiplet. Information on the corresponding wave functions can be obtained from the authors. Although the minimization is less good for set A, we notice that it better reproduces the sequence of energy levels than set B.

Magnetic Circular Dichroism

For the symbols and formula used here we refer to two recent papers [4, 5] in which it was shown that:

(i) when the M quantum number (component of the total angular moment along the z-axis) is still a good quantum number;

(ii) when the ground state is not degenerate and labelled by $M = 0$ (the case of $^7F_0$ in Eu^{3+}); and

(iii) when the excited state is doubly degenerate, the A_1-parameter is given simply by:

$$A_1 = 2|\langle J0|O_{-1}|J'M'\rangle|^2(\langle J'M'|L_z + 2S_z|J'M'\rangle)$$

where $\langle 1^N \psi JM| = \langle JM|$, the wave function for the ground state; $|1^N \psi' J'M'\rangle = |J'M'\rangle$, the wave function for the excited state; O_ρ = the transition operator with $\rho = -1$ for lcp (left circularly polarized light) and $\rho = +1$ for rcp (right circularly polarized light) and $H'_{\text{Zeeman}} = \beta H(L_z + 2S_z)$, the Zeeman Hamiltonian.

When a single M-value is no longer satisfactory for characterizing the crystal field level, the wave

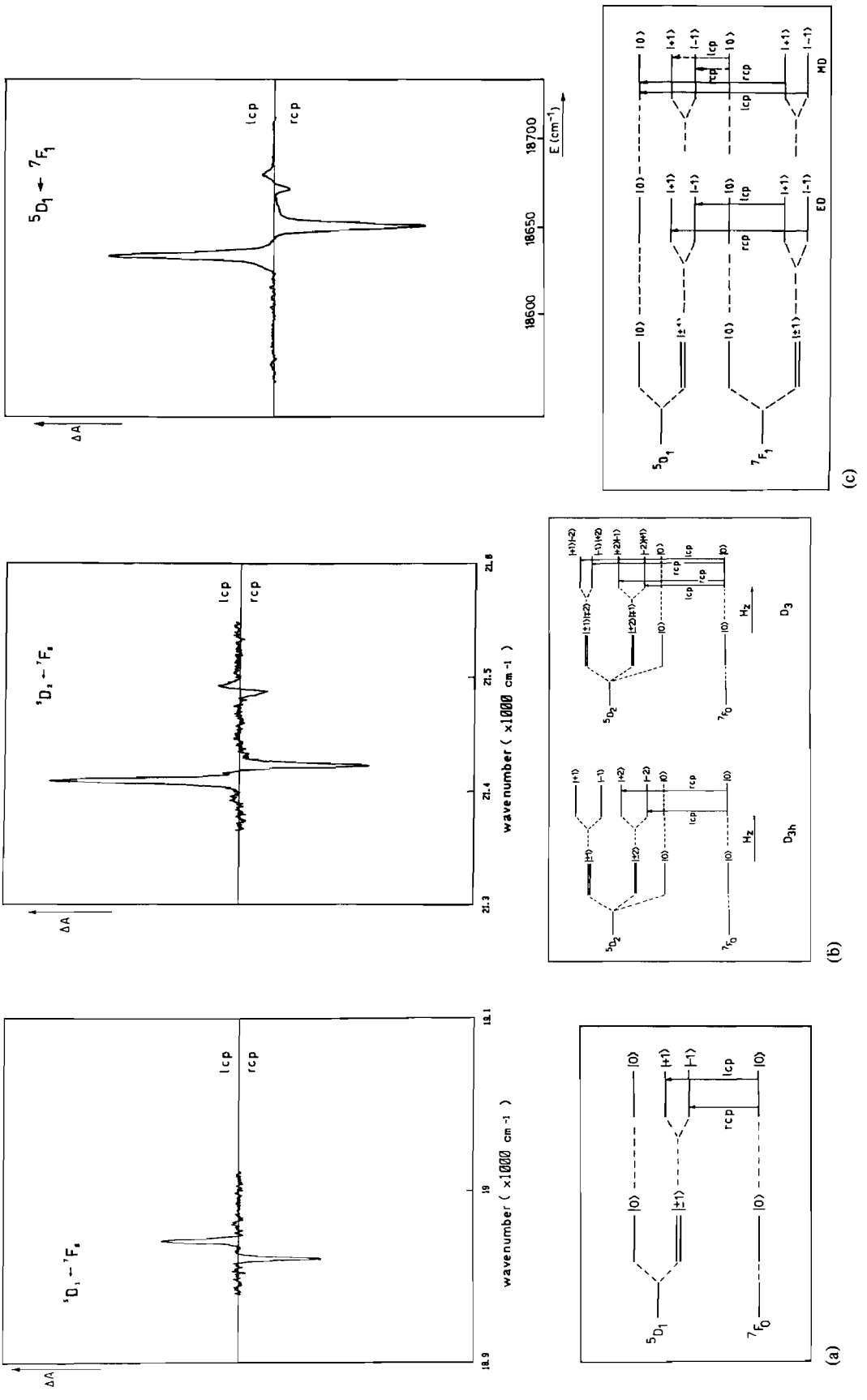
$^5D_1 \leftarrow {}^7F_1$
lcp
rcp
ΔA
E (cm^{-1})
18700
18650
18600
$^5D_2 \leftarrow {}^7F_1$
$^5D_1 \leftarrow {}^7F_1$
wavenumber (x1000 cm^{-1})
21.6
21.5
21.4
21.3
19.1
19
18.9
(a)
(b)
(c)
$^5D_1$
$^7F_0$
$^5D_2$
$^7F_1$
D_{3h}
D_3
Hz
MD
ED

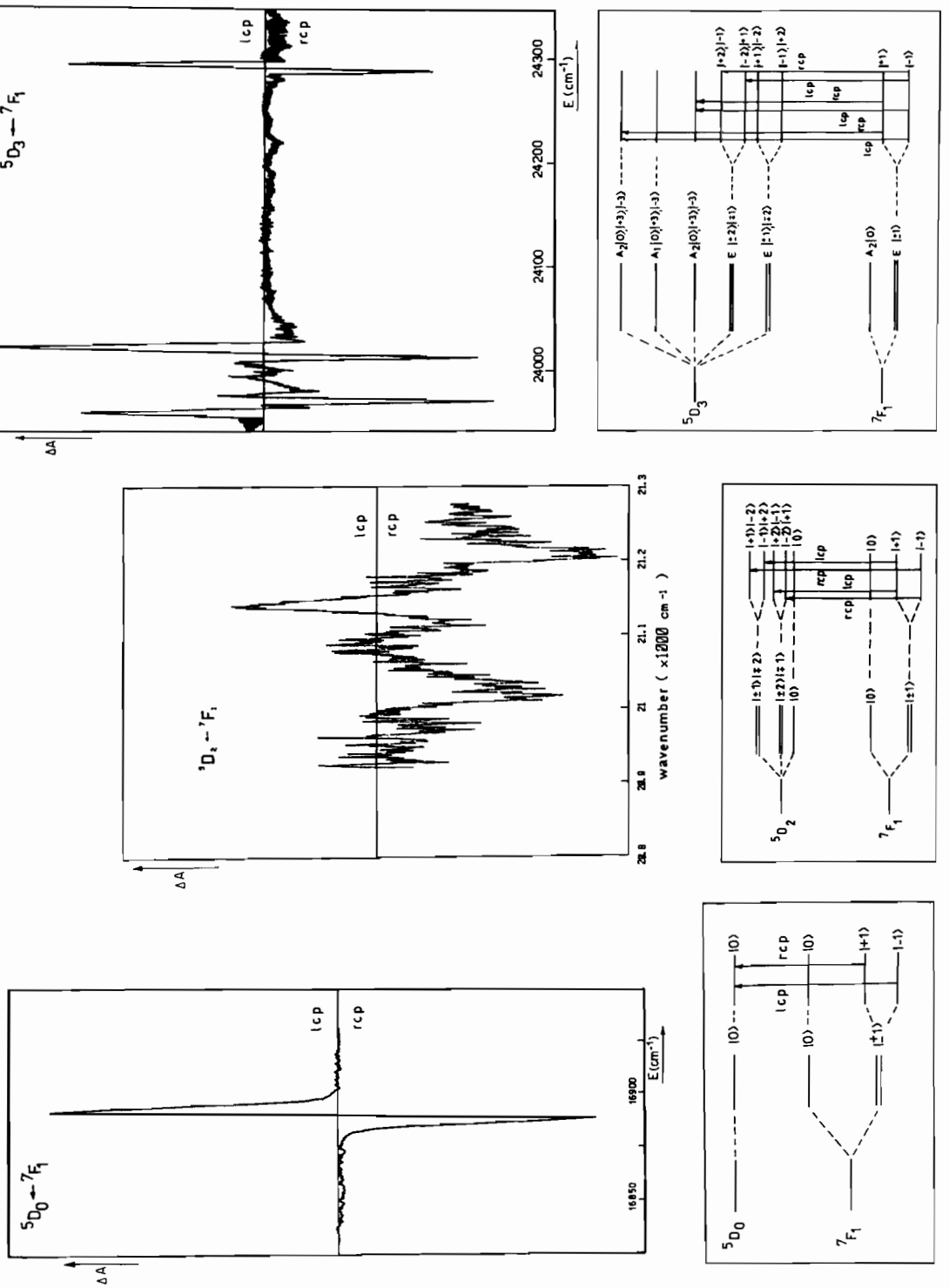

Fig. 4. MCD spectra (magnetic field = 7 Tesla, temperature = 77 K). (a): $^5D_1 \leftarrow {}^7F_0$; (b): $^5D_2 \leftarrow {}^7F_0$; (c): $^5D_1 \leftarrow {}^7F_1$; (d): $^5D_0 \leftarrow {}^7F_1$; (e): $^5D_2 \leftarrow {}^7F_1$; (f): $^5D_3 \leftarrow {}^7F_1$.

TABLE V. Free Ion and Crystal Field Parameters Calculated by the Lattice Sum Procedure (set A) and the Descending Symmetry Procedure (set B)

Free ion parameters (in cm^{-1}):			
E^0 =	2917	α =	20
E^1 =	5544	β =	−640
E^2 =	24.8	γ =	1750
E^3 =	585	ζ =	1295
(A) D_3-parameters (lattice sum)			
B_0^2 =	467		
B_0^4 =	−1007		
B_3^4 =	−936		
B_0^6 =	516		
B_3^6 =	1902		
B_6^6 =	520		
(b) D_3-parameters (descending symmetry)			
B_0^2 =	493		
B_0^4 =	−1809		
B_3^4 =	−677		
B_0^6 =	−488		
B_3^6 =	788		
B_6^6 =	860		

function for ground and excited states are written as linear combinations:

$$\langle A| = \sum_M a_M^* \langle JM|$$

$$|A'\rangle = \sum_{M'} a_{M'} |J'M'\rangle$$

These combinations are used in the expressions of the A_1-parameter [4].

In the previous papers it was also shown that the selection rules in MCD are as follows:

(i) for a magnetic dipole transition:

$$\Delta M = M' - M = -\rho$$

with $\rho = \pm 1$ for right and left circularly polarized light;

(ii) for an induced electric dipole transition:

$$\Delta M = M' - M = -\rho - q$$

with q = odd component in the expansion of the crystal field potential.

By using the crystal field Hamiltonian

$$\mathcal{H}'_{D_3(\text{odd})} = B_3^3(C_{-3}^{(3)} + C_{+3}^{(3)}) + B_3^5(C_{-3}^{(5)} + C_{+3}^{(5)}) + B_3^7(C_{-3}^{(7)} + C_{+3}^{(7)}) + B_{+6}^7(C_{-6}^{(7)} + C_{+6}^{(7)})$$

and the ordering of $\pm M'$ quantum numbers according to the crystal quantum numbers μ [15], one obtains the selection rules for magnetic and electric dipole mechanisms in circularly polarized light, given in Table VII.

TABLE VI. Observed and Calculated Energy Levels with Set A (lattice sum) and Set B (descending symmetry)

	$E_{(\text{experiment})}$	Set A		Set B	
		$E_{(\text{Theoret.})}$	Δ	$E_{(\text{Theoret.})}$	Δ
$^7F_0$	0	0.2	0	0.4	0
$^7F_1$	323	327	4	330	7
	453	447	−6	439	−14
$^7F_2$	931	925	−6	935	4
	1049	1057	8	1053	4
		1139		1285	
$^7F_3$	1821	1827	6	1832	11
		1915		1851	
	1939	1917	−22	1931	−8
	1965	1980	15	1975	10
	2063	2072	9	1984	−79
$^7F_2$		2271		2476	
	2536	2529	−7	2530	−6
	2596	2604	8	2601	5
	2907	2911	4	2859	−48
		2979		2910	
	3009	3004	−5	3014	5
$^7F_6$		4855		4807	
	4863 (E)	4859 (E)	−4	4857 (E)	−6
	4893 (E)	4894 (E)	−1	4890	−3
	4905	4911	6	4909 (E)	4
		5029		5065	
	5087 (E)	5072 (E)	−15	5074 (E)	−13
	5166 (E)	5187 (E)	21	5170 (E)	4
	5353	5336	−17	5354	1
		5337		5354	
		σ = 12.5		σ = 10.7	
Number of levels		21		21	

We shall now discuss some transitions, emphasizing the MCD contribution in the assessment of electronic transition and the identification of electronic states.

$^5D_1 \leftarrow {}^7F_0$ (Fig. 4a)

For this magnetic dipole transition a positive A_1-term is found at the wave number of the peak in the α polarization spectrum. The Zeeman component responsible for the absorption of left circularly polarized light is mainly a combination of the following $^{2S+1}L_{\chi J|M\rangle}$ wave functions

$$-0.700\ {}^5D_{31}|+1\rangle + 0.594\ {}^5D_{11}|+1\rangle + 0.216\ {}^7F1|+1\rangle - 0.195\ {}^3P61|+1\rangle - 0.168\ {}^3P31|+1\rangle$$

with χ an additional quantum number which allows characterization of the different $^{2S+1}$L-states. As the absorption of left circularly polarized light is due to the highest Zeeman component, a positive A-term

TABLE VII. Selection Rules for Electric (ED) and Magnetic (MD) Dipole Transitions in D_3 for Circularly Polarized Light (lcp = left; rcp = right)

ED	$\mu = 0$	$\mu = +1$	$\mu = -1$
	+6	+7	−7
	−6	−5	+5
	+3	+4	−4
	−3	−2	+2
	0	+1	−1
$\mu =$ 0 +6, −6, +3, −3, 0		lcp	rcp
$\mu = +1$ +7, −5, +4, −2, +1	rcp		lcp
$\mu = -1$ −7, +5, −4, +2, −1	lcp	rcp	

MD	$\mu = 0$	$\mu = +1$	$\mu = -1$
	+6	+7	−7
	−6	−5	+5
	+3	+4	−4
	−3	−2	+2
	0	+1	−1
$\mu =$ 0 +6, −6, +3, −3, 0		lcp	rcp
$\mu = +1$ +7, −5, +4, −2, +1	rcp		
$\mu = -1$ −7, +5, −4, +2, −1	lcp		

is predicted and indeed found experimentally (see Fig. 4a).

$^5D_2 \leftarrow {}^7F_0$ (Fig. 4b)

This transition is mainly electric dipole induced. Experimentally two A_1-terms are detected; a negative one at shorter wave number and a positive one at longer wave number (21 418 and 21 489 cm^{-1}).

From a consideration of the selection rules, it is seen that because $q = \pm 3$, absorption of left circularly polarized light occurs due to the $|-2\rangle$ component.

As found from the wave functions, $M' = -2$ characterizes essentially the lowest component corresponding to the E level at short energy, whereas the opposite is the case for the E component at higher energies. In the first case a negative A_1-term is predicted, in the second case the opposite holds true as is confirmed experimentally. Moreover, it is interesting to look at this in the framework of the distortion pattern $D_{3h} \rightarrow D_3$ (see Fig. 4b). In D_{3h} the lower E-state correlates to E′ corresponding only the $M' = \pm 2$ wavefunctions. In D_{3h} only absorption occurs due to this E′ level leading to a negative A_1-term. The other A_1-term is absent in the case of D_{3h} symmetry as no q-value induces this transition. The relative magnitude of the two A_1-terms in D_3 is thus a measure of the distortion $D_{3h} \rightarrow D_3$, reflected by the composition of the wave functions that in D_3 mixes in $|\pm 2\rangle$ and $|\mp 1\rangle$.

TABLE VIII. Identification of the A_1-terms Corresponding to the MCD Signals

Energy	Sign A-term	Mechanism	Identification
16892	$A(+)$	MD	$^5D_0 \leftarrow {}^7F_1$ $A_1 \leftarrow E$
18642	$A(-)$	ED	$^5D_1 \leftarrow {}^7F_1$ $E \leftarrow E$
18678	$A(+)$	MD	$A_2 \leftarrow E$
18965	$A(+)$	MD	$^5D_1 \leftarrow {}^7F_0$ $E \leftarrow A_1$
21086	$A(+)$	ED	$^5D_2 \leftarrow {}^7F_1$ $E \leftarrow E$
21164	$A(-)$	ED	$E \leftarrow E$
21418	$A(-)$	ED	$^5D_2 \leftarrow {}^7F_0$ $E \leftarrow A_1$
21489	$A(+)$	ED	$E \leftarrow A_1$
23969	$A(-)$	ED	$E \leftarrow E$
24021	$A(+)$	ED	$^5D_3 \leftarrow {}^7F_1$ $A_2 \leftarrow E$
24295	$A(+)$	ED	$A_2 \leftarrow E$

$^5D_1 \leftarrow {}^7F_1$ (Fig. 4c)

This transition is allowed by both induced electric and magnetic dipoles. No definite assessment can be made on the basis of the absorption spectrum. Experimentally one intense negative A_1-term is found at the place of the $E \leftarrow E$ transition, while a much weaker positive A_1 term appears for the $A_2 \leftarrow E$ transition.

In view of the selection rules that are illustrated in Fig. 4c, it is clear that the most intense signal is due to an induced electric dipole mechanism. That the positive A_1 term due to a magnetic dipole mechanism is much weaker is explained by the fact that:

(i) magnetic dipole intensities are weaker;

(ii) as appears from the figure, the Zeeman splitting of two E states is taken into account in the electric dipole MCD signal, while only one E state is involved in the magnetic dipole signal.

$^5D_0 \leftarrow {}^7F_1$ (Fig. 4d)

The expected positive A_1-term for this magnetic dipole transition is indeed found experimentally.

$^5D_2 \leftarrow {}^7F_1$ (Fig. 4e)

Although the signals are weak and noisy, Fig. 4e shows a positive A_1-term at the lowest energy and a negative one at the higher energy.

It is interesting to compare Fig. 4b ($^5D_2 \leftarrow {}^7F_0$) and Fig. 4e ($^5D_2 \leftarrow {}^7F_1$).

The distortion $D_{3h} \rightarrow D_3$ is clearly reflected by these transitions, but because of the different starting levels in the two cases the sequence of the A_1-terms is reversed.

$^5D_3 \leftarrow {}^7F_1$ (Fig. 4f)

In $^5D_3$ the non-degenerate A_1 level and two A_2 levels are combinations of the $|0\rangle$, $|+3\rangle$ and $|-3\rangle$ components. Starting from the E level in $^7F_1$, three positive A_1-terms are predicted. Referring to the

absorption data two of these terms ($A_2 \leftarrow E$) should be comparable in magnitude.

The E levels originating from $^5D_3$ are comparable to the E levels from $^5D_2$ and the same pattern is expected as for $^5D_2 \leftarrow {}^7F_1$. In fact only the negative term is evident in the spectrum.

A summary of the identification of MCD signals is given by Table VIII.

Conclusions

The detailed absorption, fluorescence and MCD spectra of the $YAl_3(BO_3)_4/Eu^{3+}$ crystal are discussed. The levels are simulated by a six-set crystal field parameters. Special emphasis is put on the power of the MCD technique in characterizing the wave functions corresponding to the crystal field energy levels and in assessing the intensity mechanisms responsible for transitions between these energy levels.

Acknowledgements

This work was supported through grants from the IWONL and FKFO, Belgium. The authors are indebted to the Belgian Government (Programmatie van het Wetenschapsbeleid). Travel support afforded by NATO Research grant no. 84-191 to W.T.C. and C.G.-W. is also gratefully acknowledged.

References

1 F. Kellendonk and G. Blasse, *J. Phys. Chem. Solids, 43* (5), 481 (1982).
2 F. Kellendonk and G. Blasse, *J. Chem. Phys., 75* (2), 561 (1981).
3 S. Colak and W. K. Zwicker, *J. Appl. Phys., 54* (5), 2156 (1983).
4 C. Görller-Walrand, M. Behets, P. Porcher and I. Laursen, *J. Chem. Phys., 83* (1) 4329 (1985).
5 C. Görller-Walrand and L. Fluyt-Adriaens, *J. Less-Common Met., 112*, 175 (1986).
6 M. J. M. Leask, K. J. Maxwell and B. M. Wanklyn, *J. Chem. Phys., 47* (9), 3665 (1967).
7 'Syntex XTL Users' Manual', Cupertino, Calif., 1975.
8 J. M. Stewart, P. A. Machin, C. W. Dickinson, H. L. Ammon, H. Heck and H. D. Flack, 'The X-ray System of Crystallographic Programs', Technical Report TR-446, Computer Science Center, University of Maryland, 1976.
9 C. K. Johnson, 'ORTEP', Technical Report ORNL-3974, Oak Ridge National Laboratory, Tennessee, 1965.
10 C. Görller-Walrand and P. Vandevelde, *Chem. Phys. Lett., 122* (3), 276 (1985).
11 W. T. Carnall, G. L. Goodman, R. S. Rana, P. Vandevelde, L. Fluyt and C. Görller-Walrand, *J. Less-Common Met., 116*, 17 (1986).
12 C. A. Morrison and R. P. Leavitt, *J. Chem. Phys., 71* (6), 2366 (1979).
13 R. P. Leavitt, C. A. Morrison and P. E. Wartman, 'HPL-Report, TR-1673', 1975.
14 P. Porcher, D. R. Svoronos, M. Leskelän and J. Hölsä, *J. Solid State Chem., 46*, 101 (1983).
15 B. G. Wybourne, 'Spectroscopic Properties of Rare Earths', Interscience, New York, 1965.